Supporting Information

Kounovsky-Shafer et al. 10.1073/pnas.1711069114

SI Methods

PDMS Replication of the Master Device. PDMS (Sylgard 184; Dow Corning) replicas were formed by pouring PDMS with a 10:1 ratio (wt/wt) of prepolymer to platinum catalyst and cured at 65 °C for 24 h. PDMS devices were plasma treated with O_2 (100 W, ~0.67 mbar, 36 s, GMBH 440; Technics Plasma) to produce hydrophilic channels and stored in ultrapure water for 24 h. Additionally, the treated devices were sonicated in 0.5 M EDTA, pH 8.5, for 30 min to extract Pt^+ ions (present in the PDMS catalyst), because Pt^+ ions attenuate YOYO-1/DNA fluorescence by displacing intercalated YOYO-1 with Pt^+ (1). The devices were rinsed five times in ultrapure water and rocked at room temperature for each rinse. Finally, PDMS devices were mounted on cleaned glass surfaces as previously described (2).

Adeno, pXba, Lambda, and *M. florum* DNA Preparation, Labeling, and Mapping. *M. florum* genomic DNA was prepared in gel inserts (3), nicked at Nt.BspQI restriction enzyme sites, then labeled by *Escherichia coli* polymerase I nick translation using fluorochrome-labeled nucleotides (Alexa Fluor 647) following our previously reported nanocoding protocol (1). (DNA samples were then also restriction digested with SmaI and ApaI for creating populations of linear molecules that would also support complete mapping of the *M. florum* genome.) Thus labeled molecules were stained with YOYO-1 and presented as dumbbells (4) via parking (20 V) and loading (70 V; Fig. 3) within the nanofluidic devices (Fig. 1). Restriction sites were imaged as red punctates against a green DNA backbone, revealed by FRET using laser excitation of the intercalated YOYO-1 dye (donor), which nonradiatively transfers energy to Alexa 647 fluors (acceptor) covalently incorporated within a DNA molecule. FRET imaging advantageously simplifies image acquisition by requiring just one excitation source, while also minimizing background fluorescence from unincorporated fluors (1). A restriction map, or an Nmap, of an individual DNA molecule was constructed by distance measurements (pixels) using ImageJ software (5) between centroids determined at punctates, which labeled restriction sites. Fragment sizes (kb) were then estimated by multiplication of pixel lengths by a conversion factor (kb per pixel), which also provided an apparent DNA stretch (X/L = 0.85; full length, X/L = 1) after optimization of the pairwise alignment rate of the Nmap dataset (906 Nmaps), using SOMA software (6–8) to the *M. florum* Nt.BspQI restriction map computed from sequence. The SOMA alignment parameters incorporated expected experimental errors such as sizing, and missing, or spurious punctates and 781/906 (86%) Nmaps were aligned to the *M. florum* reference map (Fig. 5). Lambda and adeno were prepared as previously described (1) and pXba was linearized.

Microscopy and Data Acquisition for Elongated DNAs with Nanoslits. A Zeiss 135M (63× objective) coupled to an argon laser (488 nm, Spectra Physics) for excitation was used for imaging YOYO-1-stained DNA molecules. Manual Collect, laboratory software (1), controlled the Hamamatsu Orca-M camera for still images, or an Andor iXon EMCCD (Andor Technology Ltd.) camera was used to acquire movies during parking and loading. For the collection of molecules bearing punctates undergoing FRET, a filter holder with filters in two different positions was used: in position 1, YOYO-1 excitation (XF3086) and in position 2, FRET excitation of Alexa Fluor 647 (XF3076; Omega Optical, Inc.) (1).

SI Electrostatic and Brownian Dynamic Simulations

To guide the design of the device we used for DNA parking and loading within a nanoslit–microchannel network, we simulated its electrical characteristics using the following approaches and approximations. The potential distribution across the device is considered by a 2D electrostatic Poisson equation, where the microchannel–nanoslit network is modeled by an anisotropic conductivity tensor and the domain outside of PDMS has isotropic bulk buffer conductivity. Electric current continuity is assumed on buffer–PDMS border and current insulation on the bath/tank walls. Electrodes at diagonal corners of the bath are taken at certain potential difference to each other, about 20 V for parking and 70 V for loading step. The resulting potential distribution within the network represents the average potential growth over many periods of the network and does not capture complex details of microchannel to nanoslit transition through a cup, involving Debye layers and EO phenomena. To derive an anisotropic conductivity tensor of the nanoslit–microchannel network, we approximate it as a periodic resistor network in which the unit cell consists of just two "resistors": one representing the resistance of a microchannel and one of the nanoslit (Fig. S1). The value of the resistors is obtained using an analytical treatment of a 1D narrow electrolyte channel model involving Poisson–Boltzmann and Navier–Stokes system of equations (9, 10).

The network conductivity tensor is given by

$$\hat{\sigma} = \begin{bmatrix} \frac{P_x}{P_y R_m} + \frac{L_n \cos^2 \alpha}{P_y R_n}, & \frac{L_n \sin\alpha \cdot \cos\alpha}{P_y R_n} \\ \frac{L_n \sin\alpha \cdot \cos\alpha}{P_x R_n}, & \frac{L_n \sin^2 \alpha}{P_x R_n} \end{bmatrix},$$

where P_x, P_y are the periods of the network in the x- and y directions, respectively, L_n is the length of the nanoslit channel, R_n, R_m are resistances of the nanoslit and microchannel segments, respectively, and α is the nanoslit angle with positive x direction. The 1D problem for the resistances R_n, R_m is solved using the finite-element method (FEM) thought the COMSOL multiphysics package. Typical potential and electrical current distribution is shown in Fig. S1 (*Right*). For instance, for a 10-mm × 10-mm device in a 20-mm × 20-mm tank filled with 0.5 mM buffer (producing Debye layer length on the order of 30 nm) and an electrode potential difference of 70 V, about 4-V drops across the PDMS are expected. The corresponding electrical field within the microchannels is around 8 V/cm.

For a detailed electrostatic study, needed to guide the location of the electrodes and to know the value and direction of the electrostatic forces, an FEM solution is performed, where the Maxwell equations are solved numerically on the complete device. The COMSOL multiphysics package is also used for this task. The domain discretization resulted in simulations with 12.5 million degrees of freedom using second-order triangular elements and including 126 microchannels and 138,600 nanoslits. Three sets of simulations were carried out, where the location of the electrodes, positive and negative, were changed relative to each other to explore the optimal conditions, i.e., direction of the electric field and the electrostatic forces, that ensure molecular parking and loading.

Fig. S2 shows representative meshes for the 2D and 3D FE analysis. In the figure, we include representative meshes for the electrostatic (2D) and the Navier–Stokes/Nernst–Planck (3D)

simulations. A major component of the theoretical design is to be able to control, in every microchannel, the electric field angle with respect to the microchannel axial direction. This consideration is fundamental to controlling the direction that DNA molecules take under EP or EO forces. In the figure, the electrical field angle is plotted as a function of the x coordinate when the electrodes are in positions 1 and 5. Notice that for position 1, the electric field direction within the microchannels is between 25° and 30°, allowing an even control of the DNA migration across the entire device. However, if the electrode is located in position 5 the electric field angle dramatically changes from bottom to top, and in some regions the angle is even higher than 90°. Position 1 allows controlled migration and synchronized parking and loading throughout the device. This advantage ensures complete use of the device area portending high-throughput operation. For example, the device used in this work comprises 128 microchannels × 1,100 nanoslits × 28-μm-long nanoslits, which can house DNA molecules at the rate of 2.28 kb/μm (YOYO-1 stained DNA) = 8.84 Gb, which is equivalent to 2.8 human genomes per-device loading.

SI Theoretical Considerations

The contour length L_d of the DNAs is 7.7, 12.2, and 16.5 μm for pXba, adeno, and λ, respectively. The excluded volume parameter z_{el} is a measure of the excluded-volume effect and has been discussed for DNA previously by us (4). Here, it is close to unity for all three DNAs. We may then compute the radii of gyration of the respective DNAs and they turn out to be close to the height H ≃ W ≃ 1.7 μm or smaller. The DNA coils as such fit in the cups fairly easily.

Next, an electric field $\vec{E}$ is applied to the DNA within the microchannel cup, momentarily assuming the molecule does not leak into the nanochannel. The total free energy of the DNA may be written as

$$\frac{F_{tot,m}}{k_BT} \simeq \frac{R_o^2}{R_c^2} + \frac{\beta N_p^2}{H^2 R_c} + \frac{N_e e E R_c}{k_BT}, \qquad \textbf{[S1]}$$

neglecting numerical coefficients. The first term arises from the entropy of compressing the (ideal) DNA into a box of size $R_C H^2$, where R_C signifies the thickness of compression of the DNA coil. The initial radius R_o of extension of the chain equals $\sqrt{2L_d l_p}$; the first term is proportional to R_o^2 because it must be extensive. The second term represents the excluded-volume effect with $N_p = L_d/l_p$ segments of length l_p interacting with each other within a volume $R_C H^2$. The excluded volume β between two segments scales as $l_p^2\omega$, where ω is the effective diameter of the DNA helix. The last term in Eq. **S1** is the electrostatic energy of the DNA chain in the electric field. It is assumed that the usual condition of counterion condensation is applicable. The DNA thus bears $N_e = L_d/Q$ elementary charges where $Q = e^2/4\pi\varepsilon_o\varepsilon_r k_BT = 0.71$ nm is the Bjerrum length. At $R_c \simeq H$, the first two terms in Eq. **S1** are of the same order of magnitude as has been argued above ($z_{el} \simeq 1$). Upon substantial compression of the coil, the first term overwhelms the second. Therefore, minimization of $F_{tot,m}$ with respect to R_c leads to

$$R_c^3 \simeq \frac{l_p^2 Q}{\alpha}, \qquad \textbf{[S2]}$$

$$F_{tot,m} \simeq \alpha^{2/3}\left(\frac{L_d}{l_p^{1/3}Q^{2/3}}\right), \qquad \textbf{[S3]}$$

if the electric field is high enough (i.e., $R_c < H$). We have defined the dimensionless parameter

$$\alpha \equiv \frac{l_p e E}{k_BT}. \qquad \textbf{[S4]}$$

At low E, R_c would be close to R_o, so the third term in Eq. **S1** would be merely perturbative.

A convenient unit of magnitude of the electric field in our experiments is $E_1 = 1$ V/cm. The parameter α then has the very small magnitude

$$\alpha_1 = \frac{l_p e E_1}{k_BT} \simeq 4.4\times10^{-4}. \qquad \textbf{[S5]}$$

At $E = 10\ E_1 = 10$ V/cm, say, the radius of compression R_c is about 1 μm, so the electric field clearly starts having an impact on the size of the DNA coil in that case.

If we suppose the DNA molecule had entered the nanochannel entirely, but with one end fixed at the junction with the microchannel, its free energy would be

$$\frac{F_{tot,n}}{k_BT} = \frac{c_1 L_d}{l_p^{1/3}}\left(D^{-2/3} + h^{-2/3}\right) - \frac{N_e e E L_d}{2k_BT}. \qquad \textbf{[S6]}$$

The first term is the free energy of confinement based on Burkhardt's analysis and discussed previously (4) for a nanoslit of width D and height H; the coefficient $C_1 = 1.1036$. The second term is the electrostatic energy of the DNA under the influence of the electric field. The macromolecule is approximated as a straight rod of length L_d bearing N_e elementary charges.

At large enough $E > E_*$, the DNA can no longer reside in the microchannel [$F_{tot,m}(E_*) = F_{tot,n}(E_*)$]. At electric fields with $E > E_*$, there is a barrier given by $\Delta F = F_{tot,n} - F_{tot,m}$. In the latter case, within transition-state theory (11), the rate of escape of the DNA from the microchannel cup would be expressed by a dynamic front factor times a Boltzmann factor exp − ($\Delta F/k_BT$). The DNA is assumed to be in equilibrium because the time scale of relaxation of the DNA segments is much smaller than that associated with the escape time into the nanochannel. Within this admittedly crude scenario, parking of the DNA coil would occur at $E < E_*$. Once the DNA molecule passes the barrier into the nanochannel, it moves further along in the latter owing to the electric field.

Within the context of this scenario, the loading efficiency $L_{p,E} = 0$ occurs at $\Delta F \simeq 0$, that is, at $E = E_*$. The electrodes are separated by a distance of 2.5 cm. Eqs. **S3**, **S5**, and **S6** lead to

$$0.2Z_* + C_2\left(\frac{l_p^2 Q}{\alpha_1 L_d^2}\right)^{1/3}(0.4Z_*)^{2/3} \simeq \frac{Q l_p^{2/3}}{\alpha_1 h^{2/3}}, \qquad \textbf{[S7]}$$

$$Z_* \equiv V_{L,*} L_d. \qquad \textbf{[S8]}$$

Here, V is given in volts and C_2 is a constant of order unity. The second term on the left-hand side of Eq. **S7** is generally small, so we conclude that Z_* must be basically a constant.

SI EO Flow Experiments with DNAs, Beads, and Rhodamine Dye

Ionic Strength Affects DNA Migration Within the Microchannel/Nanoslit Device. DNA molecules in different ionic strength (IS) conditions [IS = 0.5 mM (0.05× TE) or 8.5 mM (1× TE); pH = 7.9] were used to test how IS conditions affect the EO flow in microchannels (Fig. 2 *A* and *B*). DNA molecules were loaded into the microchannel via capillary flow, the device was immersed in buffer, and then an electric field was applied (Fig. 1). Two different devices are utilized in this experiment (Fig. S3): the device described here and a device with only microchannels

(100 μm wide × 3.3 μm high; ref. 2). The IS was varied to the direction that DNA migration takes to inform the contributions of EO and EP flows within microchannels. A voltage of 20 V was applied to the device and molecules were imaged using an SIT camera connected to Pinnacle Studio software. Molecules were analyzed using ImageJ software to track the centroid position of the molecule.

At lower IS environments, the migration in the microchannel is acute—EO flow dominates. At high IS conditions, EP forces dominate.

Carboxyl-Terminated or Native Polystyrene Beads. Carboxyl-terminated beads (0.11-μm diameter; Molecular Probes) and native polystyrene beads (0.11-μm diameter; Polysciences) were diluted in 0.5 mM NaCl, pH = 6.4, for subsequent analysis of EO flow in the microchannel. Beads were loaded into the microchannels through capillary loading; then, the entire device was immersed in buffer (0.5 mM NaCl, pH = 6.4), the Plexiglas holder was mounted to the microscope stand, and the power supply was attached to the electrodes. Beads were electrokinetically moved (20 V) within microchannels to check the loading direction: obtuse (dominated by EP) or acute (dominated by EO). Both sets of beads, carboxyl-terminated (Fig. S4*A*) and native polystyrene beads (Fig. S4*B*), migrated in the microchannel with acute loading (via EO flow) under low IS, which is in the same direction as the DNA molecules, indicating that EO flow dominates in the microchannels. The diluted beads, carboxyl-terminated or native polystyrene, were imaged in the microchannels using an Andor iXon camera with a frame rate ∼15 frames per second and tracked over time using ImageJ (5).

Rhodamine B Dye. A plug of 0.9 mM Rhodamine B (Thermo Fisher Scientific) dye (pH 4.7) was formed within the microchannels to elucidate EO flow. To form a plug, water was introduced into the device, then the excess water (water outside the device) was removed, Rhodamine B sample was added to an entrance, on the other side of the device; an aspirator was used to remove some of the water, and finally the device was immersed in water. A voltage (50 V) was applied to the device causing dye migration in microchannels, which were imaged using an SIT 68 camera coupled to a Pinnacle Studio video digitizer, controlled by a computer. Resulting movies were manually analyzed for tracking dye migration patterns (Fig. S4*C*). The movement of the Rhodamine toward the anode indicates EO forces.

Zeta-Potential Measurements of Carboxyl-Terminated or Native Polystyrene Beads. Native and carboxyl-terminated polystyrene beads (0.11 μm) were purchased from Polyscience and Invitrogen, respectively. The zeta potentials of native polystyrene beads, and carboxylated polystyrene beads were measured and referenced against a standard solution (68 ± 6.8 mV; Malvern Instruments) using a Zetasizer Nano ZS instrument (Malvern Instruments). Native and carboxyl-terminated polystyrene beads were diluted using distilled, autoclaved, and filtered water (0.2-μm filter), and then brought up to 0.5 mM NaCl.

1. Jo K, et al. (2007) A single-molecule barcoding system using nanoslits for DNA analysis. *Proc Natl Acad Sci USA* 104:2673–2678.
2. Dimalanta ET, et al. (2004) A microfluidic system for large DNA molecule arrays. *Anal Chem* 76:5293–5301.
3. Schwartz DC, Cantor CR (1984) Separation of yeast chromosome-sized DNAs by pulsed field gradient gel electrophoresis. *Cell* 37:67–75.
4. Kounovsky-Shafer KL, et al. (2013) Presentation of large DNA molecules for analysis as nanoconfined dumbbells. *Macromolecules* 46:8356–8368.
5. Abramoff MD, Magelhaes PJ, Ram SJ (2004) Image Processing with ImageJ. *Biophoton Int* 11:36–42.
6. Teague B, et al. (2010) High-resolution human genome structure by single-molecule analysis. *Proc Natl Acad Sci USA* 107:10848–10853.
7. Valouev A, et al. (2006) Alignment of optical maps. *J Comput Biol* 13:442–462.
8. Sarkar D, Goldstein S, Schwartz DC, Newton MA (2012) Statistical significance of optical map alignments. *J Comput Biol* 19:478–492.
9. Levine S, Marriott JR, Robinson K (1975) Theory of electrokinetic flow in a narrow parallel-plate channel. *J Chem Soc Faraday Trans II* 71:1.
10. Stein D, Kruithof M, Dekker C (2004) Surface-charge-governed ion transport in nanofluidic channels. *Phys Rev Lett* 93:035901.
11. Zwanzig R (2001) Reaction rates. *Nonequilibrium Statistical Mechanics* (Oxford Univ Press, New York), pp 67–82.

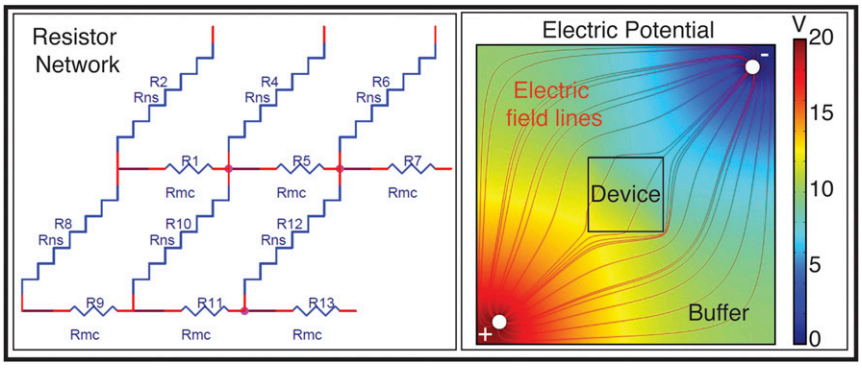

Fig. S1. (*Left*) Resistor network approximation for nanoslit–microchannel network. Unit cell consists of one resistor representing microchannel resistance and one resistor representing the nanoslit. The value of the resistors can be obtained from 1D narrow electrolyte channel model involving Poisson–Boltzmann and Navier–Stokes system of equations. (*Right*) Potential and electric field lines within the device and tank when a potential difference of 20 V is applied.

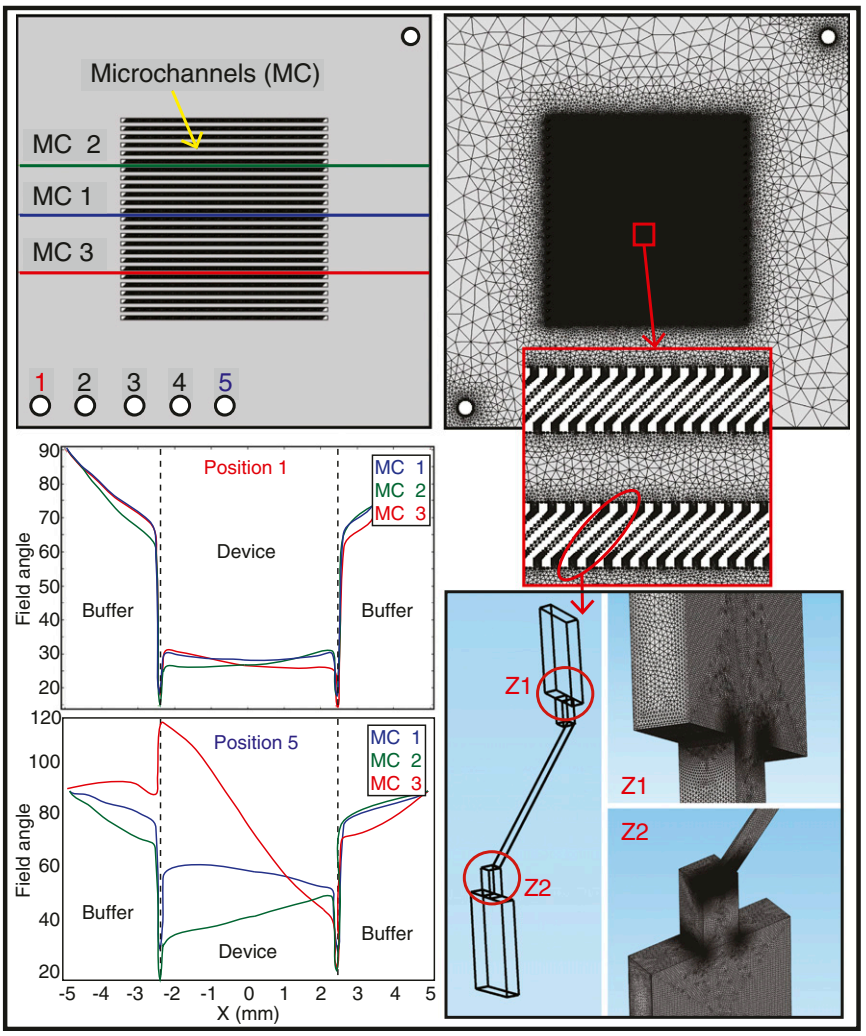

Fig. S2. Two levels of FE simulations to aid the device design. The device domain is discretized for 2- and 3D analysis including the full electrostatic details (potential, field, forces) and Navier–Stokes/Nernst–Planck molecular simulations. Representative meshes for both studies are included. A major component of the design is the angle of the electrical field with respect to the microchannel axial direction. This angle controls the direction of the EP and EO forces. The location of the electrodes was selected based on this angle, which is shown for the locations 1 and 5 of the electrode.

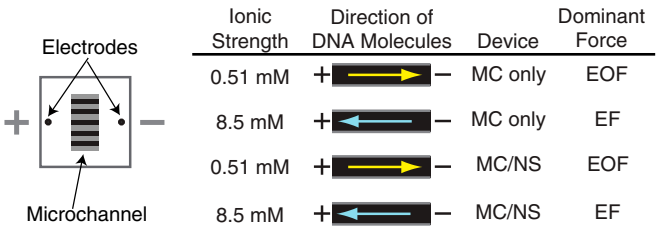

Fig. S3. Summary of DNA loading dynamics affected by IS—"middle electrode." Using a middle electrode conformation, migration of adeno DNA molecules (39.5 kb) is dominated by EP or EO forces when driven through a microchannel device (MC, without nanoslits; 100 μm wide × 3.3 μm tall), or a microchannel–nanoslit device (MC/NS), under different ionic strength conditions: 0.06× TE (I = 0.51 mM) or 1× TE (I = 8.5 mM). Depending on the IS, EO or EP forces will dominate. With the side electrode conformation, the loading regime for low or high IS solutions is acute or obtuse loading, respectively. Acute loading is dominated by EO flow, while EP forces dominate obtuse loading. Yellow and blue arrows indicate EO flow and EP flow, respectively. (n = 30 measurements).

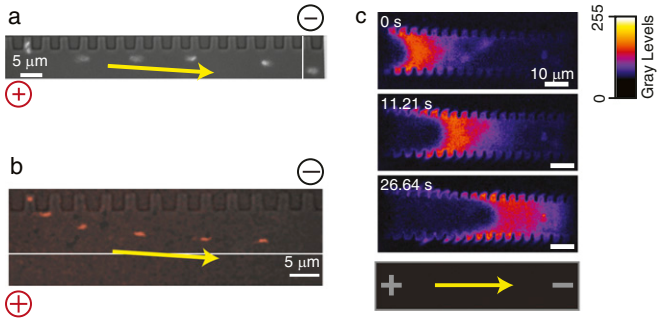

Fig. S4. Loading dynamics of Rhodamine B dye, native, and carboxyl-terminated polystyrene microspheres. (*A* and *B*) Using a side electrode conformation ("+," "−" show electrode orientation and polarity) fluorescently labeled carboxyl-terminated (*A*) or native (*B*) polystyrene microspheres are electroosmotically driven through the microchannel–nanoslit device. Images in *A* and *B* are multiple images superimposed into one image to document the progression of a bead in the microchannel. The time between each image is 0.5 s for *A* and 0.6 s for *B*. (*C*) Neutral Rhodamine B dye migrates electroosmotically in the microchannel of the microchannel–nanoslit device. A DIC image of the microchannel–nanoslit device is overlaid on top of the fluorescence micrographs. A color look-up table is shown to the right of the image. Yellow arrows indicate EO flow.

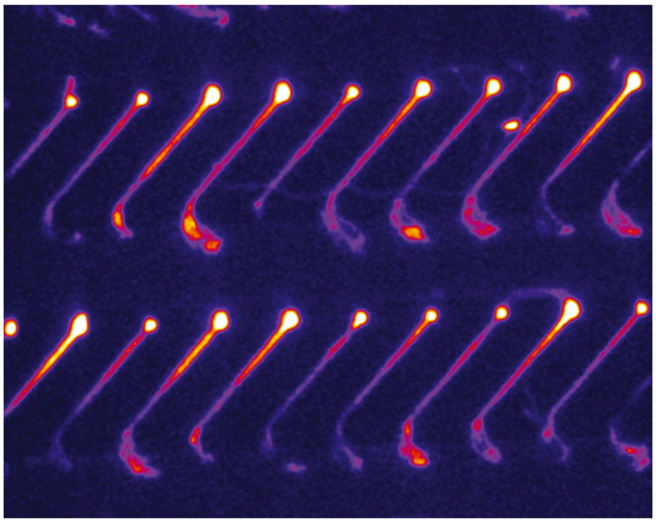

Movie S1. Parking and loading of T4 DNA molecules to form a plethora of DNA dumbbells is shown. DNA molecules are parked in molecular gates, which are abutted next to nanoslits, under a low voltage (V_p = 20 V). DNA molecules are triggered to load at a higher voltage (V_L = 70 V) to form dumbbells. Original movie duration is 70.0 s (~214 ms per frame), but is compressed here to run 4.38× faster; movie field is 26.9 × 21.3 μm.

Movie S1